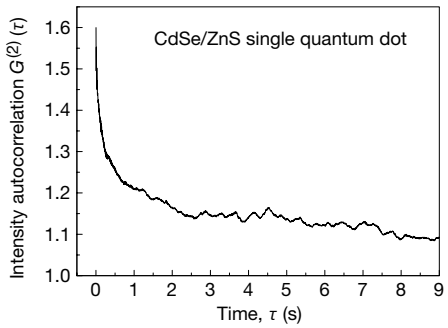

Figure 4 Intensity autocorrelation $G^{(2)}(\tau)$ obtained for the time trace shown in Fig. 3.

indication that blinking does not occur on the timescales of interest for photon antibunching.

Prior measurements on single QD photoluminescence and absorption have demonstrated the existence of discrete QD resonances[8]. However, just as the observation of discrete absorption lines in an atomic vapour cannot be taken as an evidence that the observed system consists of a single atom, these experiments, at least in principle, cannot rule out the existence of several QDs. In contrast, photon correlation measurements, such as the one reported here, provide a reliable method for deciding whether or not the observed system is a single anharmonic quantum emitter. In addition, owing to interactions with the lattice, a nanostructure that acts like an anharmonic emitter at cryogenic temperatures can be indistinguishable from a higher-dimensional system at room temperature. We have demonstrated that a CdSe quantum dot behaves as an anharmonic emitter even at room temperature. Our results constitute a first step in the study of quantum optical phenomena in semiconductor QDs. Demonstration of quantum dynamics in semiconductors at room temperature could lead to applications in quantum information processing and computation. □

Methods

Sample preparation

The CdSe/ZnS (core/shell) quantum dots were synthesized following high-temperature organometallic methods described in the literature[11–13]. The resulting nanoparticles were capped with the organic ligand trioctylphosphine oxide (TOPO) and had a distribution with an average diameter of 4.1 nm and a r.m.s. (root mean square) width of 0.33 nm (8% size distribution). The single QD samples were prepared by spin-casting 30 μl of a 0.5 nM solution of the QDs dissolved in hexanes onto a bare glass coverslip, which resulted in a mean separation of the QDs of approximately 1 μm.

Experimental set-up

Optical pumping was performed using circularly polarized light of the 488-nm line of a continuous-wave Ar^+ laser, generating electron–hole pairs in the excited states of the CdSe quantum dots. The exciting light was focused by a high numerical aperture (NA is 1.3) oil-immersion objective to a near-diffraction-limited (full-width at half-maximum (FWHM)) spot approximately 300 nm in diameter at the glass–sample interface. In order to minimize the generation of two electron–hole pairs simultaneously we used a low excitation intensity of about 250 W cm^{-2}. Typically, a QD was excited approximately every 1–10 μs (ref. 14), whereas the photoluminescence decay time is of the order of 30 ns. Thus the probability of generating two electron–hole pairs was small. The photoluminescence from the QD was collected by the same objective and first passed through the excitation laser beam splitter and then through a holographic notch filter to block scattered laser light. The light was then split with a 50/50 non-polarizing beam splitter and the resulting two photon beams were focused onto the active areas of two single-photon-counting avalanche photodiodes (SPAD).

Measurement

Photoluminescence images of the nanocrystals were obtained by scanning the QD-covered glass plate through the laser focus and recording the number of counts with one of the SPADs. To measure the photon statistics of a selected QD (or a cluster of QDs), the glass plate was positioned where a single bright spot of typically 300 nm in diameter (resolution limited) was observed in the photoluminescence image. The number of pairs of photons $n(\tau)$ with arrival-time separations of τ was measured using the two SPADs for $\tau \leqslant \tau_{max} = 200$ ns. The pulses from the two SPADs were used to start and stop a time-to-amplitude converter (TAC) where the time delay between the start and stop pulses (to within τ_{res}) was converted to a voltage amplitude. The SPADs exhibited the same counting rate. An electronic delay (53 ns) was introduced in the stop channel in order to check the symmetry of the $n(\tau)$ signal and to avoid the effect of noise for small voltages in the TAC. The output pulses were fed into a multichannel analyser. To reduce the background contribution and therefore decrease the amount of uncorrelated light in the $n(\tau)$ measurement, the multichannel analyser was enabled only during the 'on' periods, that is, when the signal level was above a certain threshold.

Received 17 April; accepted 3 July 2000.

1. Walls, D. F. & Milburn, G. J. *Quantum Optics* (Springer, Berlin, 1994).
2. Hanbury-Brown, R. & Twiss, R. Q. Correlation between photons in two coherent beams of light. *Nature* **177,** 27–29 (1956).
3. Kimble, H. J., Dagenais, M. & Mandel, L. Photon antibunching in resonance fluorescence. *Phys. Rev. Lett.* **39,** 691–694 (1977).
4. Diedrich, F. & Walther, H. Nonclassical radiation of a single stored ion. *Phys. Rev. Lett.* **58,** 203–206 (1987).
5. Basché, Th., Moerner, W. E., Orrit, M. & Talon, H. Photon antibunching in the fluorescence of a single dye molecule trapped in a solid. *Phys. Rev. Lett.* **69,** 1516–1519 (1992).
6. Fleury, L., Segura, J.-M., Zumofen, G., Hecht, B., Wild, U. P. Nonclassical photon statistics in single-molecule fluorescence at room temperature. *Phys. Rev. Lett.* **84,** 1148–1151 (2000).
7. Nirmal, M. *et al.* Fluorescence intermittency in single cadmium selenide nanocrystals. *Nature* **383,** 802–804 (1996).
8. Empedocles, S. & Bawendi, M. G. Spectroscopy of single CdSe nanocrystallites. *Acc. Chem. Res.* **32,** 389–396 (1999).
9. Klimov, V. I. & McBranch, D. W. Femtosecond 1P-to-1S electron relaxation in strongly confined semiconductor nanocrystals. *Phys. Rev. Lett.* **98,** 4028–4031 (1998).
10. Efros, Al. L. & Rosen, M. Random telegraph signal in the photoluminescence intensity of a single quantum dot. *Phys. Rev. Lett.* **78,** 1110–1113 (1997).
11. Murray, C. B., Norris, D. J. & Bawendi, M. G. Synthesis and characterization of nearly monodisperse CdE (E = S, Se, Te) semiconductor nanocrystallites. *J. Am. Chem. Soc.* **115,** 8706–8715 (1993).
12. Hines, M. A. & Guyot-Sionnest, P. Synthesis and characterization of strongly luminescing ZnS-capped CdSe nanocrystals. *J. Phys. Chem.* **100,** 468–571 (1996).
13. Dabbousi, B. O. *et al.* (CdSe)ZuS core shell quantum dots: synthesis and characterization of a size series of highly luminescent nanocrystallites. *J. Phys. Chem.* **101,** 9463–9475 (1997).
14. Nirmal, M. & Brus, L. Luminescence photophysics in semiconductor nanocrystals. *Acc. Chem. Res.* **32,** 407–414 (1999).

Acknowledgements

This work is supported by the David and Lucile Packard Fellowship (A.I. and S.K.B.). P.M. acknowledges the financial support of the Max Kade Foundation.

Correspondence and requests for materials should be addressed to A.I. (e-mail: atac@ece.ucsb.edu).

Organoplatinum crystals for gas-triggered switches

Martin Albrecht*, Martin Lutz†, Anthony L. Spek† & Gerard van Koten*‡

** Debye Institute, Department of Metal-Mediated Synthesis & † Bijvoet Center for Biomolecular Research, Crystal and Structural Chemistry, Utrecht University, Padualaan 8, 3584 CH Utrecht, The Netherlands*

Considerable effort is being devoted to the fabrication of nanoscale devices[1]. Molecular machines, motors and switches have been made, generally operating in solution[2–7], but for most device applications (such as electronics and opto-electronics), a maximal degree of order and regularity is required[8]. Crystalline materials would be excellent systems for these purposes, as crystals comprise a vast number of self-assembled molecules, with a perfectly ordered three-dimensional structure[9]. In non-porous crystals, however, the molecules are densely packed and any change in them (due, for example, to a reaction) is likely to destroy the crystal and its properties. Here we report the controlled and fully reversible crystalline-state reaction of gaseous SO_2 with non-porous crystalline materials consisting of organoplatinum molecules. This process, including repetitive expansion–reduction sequences (on gas uptake and release) of the crystal lattice, modifies the structures of these molecules without affecting their crystallinity. The process is based on the incorporation of SO_2 into the colourless crystals and its subsequent liberation from

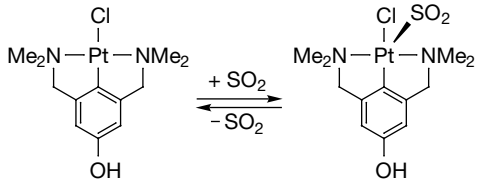

1 2

Figure 1 Reversible adsorption of SO_2 by organoplatinum(II) species containing the *N,C,N'* terdentate coordinating, monoanionic 'pincer' ligand.

the orange adducts by reversible bond formation and cleavage[10]. We therefore expect that these crystalline materials will find applications for gas storage devices and as opto-electronic switches[11,12].

Chemical transformations that occur in crystalline material, so-called 'crystalline-state reactions'[13], are very rare because most chemical reactions cause considerable stress and intermolecular reorganization. Hence, the loss of crystallinity is a typical event. Among the best explored crystalline-state reactions are (reversible) photochemical isomerization processes, that is, unimolecular, light-induced transformations in the crystal[14–16]. Processes in the crystalline phase that involve substrate binding and release, and thus a change in the overall atom content within the unit cell, have been

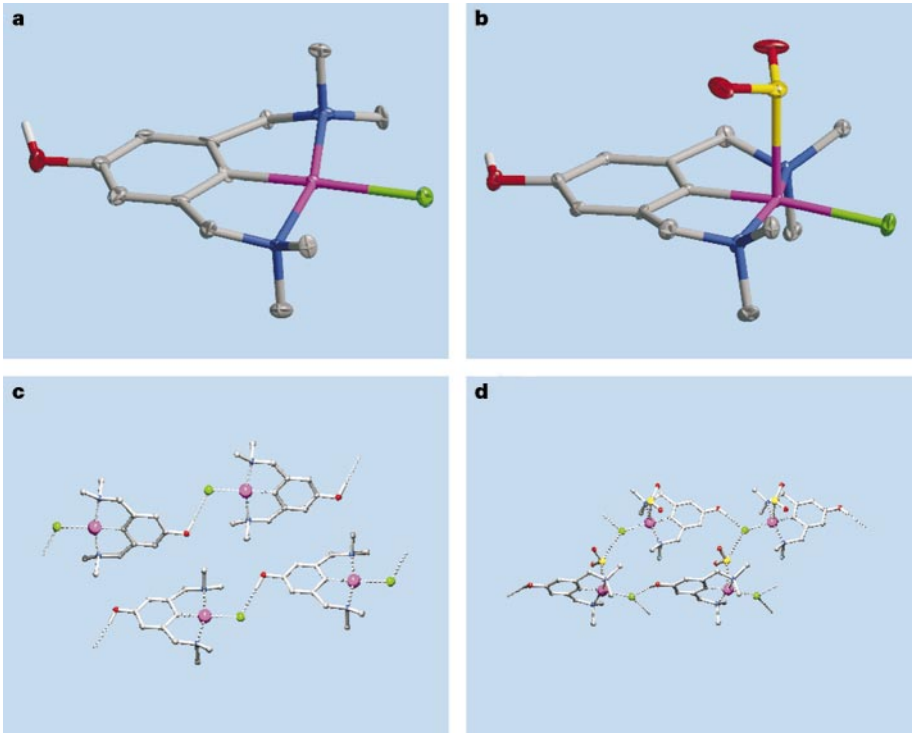

Figure 2 Molecular structures and hydrogen bonding motifs of organoplatinum complexes **1** and **2**. **a**, **b**, The molecular structures were determined by single crystal X-ray diffraction and demonstrate the change in the geometry around platinum upon coordination of SO_2: distorted square-planar in **1** (**a**) versus square-pyramidal in the adduct **2** (**b**). **c**, **d**, The α-type supramolecular connectivity pattern, that is, the Pt–Cl···H–O hydrogen bonding, is similarly present in **1** (**c**) and in **2** (**d**). The β-type network mediated by Pt···S···Cl interactions is only found in **2**. All hydrogen atoms except the phenolic O–H hydrogen have been omitted for clarity. Elements are colour-coded: platinum (purple), nitrogen (blue), chlorine (green), oxygen (red), sulphur (yellow). X-ray crystallographic details for the single crystal structure determination for **1**: intensities were measured at 150 K using graphite-monochromated Mo Kα radiation (λ = 0.71073 Å). 2,936 independent reflections (6,631 total measured) were analysed by using automated Patterson methods. Structure refinement on F^2 structure factors converged with a discrepancy factor $R_1 = 0.0376$ and a weighted discrepancy factor $wR_2 = 0.0793$ (goodness of fit = 1.024). The oxygen-bound hydrogen was located in the difference Fourier map and allowed to refine freely. Residual electron density was only found within 0.84 and –1.08 e Å^{-3}. An identical experimental set-up was used for the analysis of the adduct **2**. The structure was solved by using automated Patterson methods on 2,166 independent reflections (11,626 total measured). Structure refinement on F^2 converged at $R_1 = 0.0350$ and $wR_2 = 0.0558$ (goodness of fit = 1.054). The oxygen-bound hydrogen was located in the difference Fourier map and refined with a rotating model. Residual electron density was only found within 0.97 and –1.01 e Å^{-3} (for further details, see refs 10 and 24, respectively). Selected bond distances (in Å) and angles (in degrees) around platinum for **1**: Pt–C, 1.915(9); Pt–Cl, 2.434(2); Pt–N1, 2.094(8); Pt–N2, 2.082(8); N1–Pt–N2, 163.9(3); C–Pt–Cl, 177.4(4); and for **2**: Pt–C, 1.923(10); Pt–Cl, 2.423(3); Pt–N1, 2.106(8); Pt–N2, 2.096(8); N1–Pt–N2, 160.5(3); C–Pt–Cl, 173.1(3). (N1 and N2 are the respective nitrogen atoms, coloured blue).

Table 1 Selected crystallographic parameters of 1 and 2

Complex	Space group (number)	Unit cell dimensions				Density, ρ (g cm^{-3})	Packing index (%)
		a (Å)	*b* (Å)	*c* (Å)	*V* (Å^3)		
1 (ref. 24)	$Pna2_1$ (33)	24.2238(14)	10.1986(8)	5.4483(14)	1,346.0(4)	2.1606(6)	72.2
2 (ref. 10)	$Pna2_1$ (33)	16.837(3)	10.2189(16)	9.0231(10)	1,552.5(4)	2.1473(6)	70.9

restricted to enzymes and other materials with an 'open' (that is, porous)[17] structure with large cavities (for example, zeolites)[18–20]. A versatile way of overcoming this problem relies on crystal engineering[21], whose intention is the design and processing of supramolecular properties in solids[22].

Our approach towards the property-directed synthesis of new and well-defined materials involves the use of the *N,C,N′* terdentate coordinating, monoanionic 'pincer' ligand system $[C_6H_2(CH_2NMe_2)_2$-2,6-R-4], abbreviated as NCN-R, where R is a functional group[23]. When complexed to four-coordinated metal centres (for example, Pt(II)), the fourth site is forced to occupy a *trans* position to the metal–carbon bond, due to the chelating binding mode of the pincer ligand (Fig. 1). In addition, modification of the aryl ring of the ligand allows for the introduction of functional groups such as an acceptor or donor site. Using this method, the organoplatinum complex [PtCl(NCN-OH)] (**1**) was prepared recently[24]; it contains a metal-bound chloride as a hydrogen bond acceptor and a phenolic hydroxide group on the pincer ligand as a hydrogen donor. With this supramolecular synthon[25], the organoplatinum complex self-assembles in the solid state to form an α-type network via intermolecular Pt–Cl···H–O (hydrogen) bonds (Fig. 2).

When crystalline **1** is exposed to an atmosphere of SO_2, adsorption of this gas by the organoplatinum sites is indicated by a dramatic colour change of the material from colourless to deep orange, a colour change previously also observed in solution[10,26]. This adduct formation modifies the geometry around platinum and was therefore expected to destroy the crystallinity. Surprisingly however, exposure of crystalline **1** to SO_2 gas (about 1 minute exposure time) gives the corresponding adduct [PtCl(NCN-OH)(SO_2)], **2** (Fig. 1), in a quantitative, crystalline-state reaction. Unequivocal evidence for this process has been obtained by X-ray powder diffraction and solid-state infrared spectroscopy. Similarly, the reverse reaction in an SO_2-free environment leads to the complete regeneration of crystalline **1**.

The structural features of **1** and **2** are known from single crystal analyses taken on crystals that were grown from saturated solutions (Fig. 2a, b)[10,24]. On absorption of SO_2, the molecular structure is changed predominantly around the platinum atom. The metal centre is no longer of square-planar but of approximate square-pyramidal geometry. This has an influence on the packing index and the density, which decrease, and on the unit cell volume, which is expanded by more than 15% after absorption of SO_2 (Table 1). Intermolecular Pt–Cl···H–O hydrogen bonding in **1** results in the formation of an α-type network (Fig. 2c). Tight fixation of SO_2 in **2** occurs by a Pt···S(O)$_2$···Cl bond formation perpendicular to the hydrogen bond network[27], which results in a unusual β-type network (Fig. 2d). The distances between hydrogen bond donors and acceptors (H···Cl is 2.33(9) Å in **2** and 2.32(13) Å in **1**; O···Cl is 3.127(8) Å in **2** and 3.126(8) Å in **1**) as well as the bond angles (O–H···Cl is 165(8)° in **2** and 161(15)° in **1**) are statistically identical.

When SO_2-free organoplatinum crystals are subjected to an environment of SO_2 for a few seconds, only partial binding of the substrate is observed and a mixture of the two crystalline compounds **1** and **2** is obtained. The precise composition of this mixture is strongly dependent on the exposure time and the sample preparation. However, the powder diffraction diagram of the mixture can be used to access the ratio of **1** and **2** because their patterns are very different. Therefore, the comparison of the measured powder diagram with those simulated from the single crystal structures affords a good estimation of the ratio between **1** and **2**.

The reversibility and kinetics of these crystalline-state reactions have been elucidated by time-resolved X-ray powder diffraction[28] and infrared spectroscopy. By overlapping of the time-resolved infrared spectra, various isosbestic points have been identified which strongly suggest a direct transformation of **1** into **2** and vice versa. We examined the stretching vibrations of bound SO_2 (ν_s = 1,072 and ν_{as} = 1,236 cm^{-1}). The (dis)appearance of these

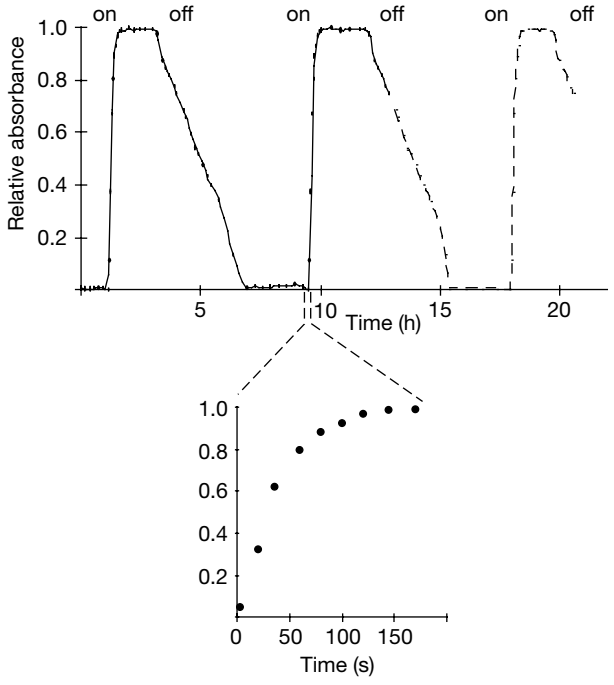

Figure 3 'On/off' switching between crystalline **1** and **2**. Switching was monitored by infrared spectroscopy in an environmental DRIFT (diffuse reflectance infrared Fourier transform) chamber. The vibration of platinum-bound SO_2 (ν_s = 1,072 cm^{-1}) is diagnostic for the position of the switch. Spectra were recorded at 293 K every 20 seconds (average of 4 scans) under a continuous flow of SO_2 (crystalline-state reaction giving **2**) and N_2 (giving **1**), respectively. Repetitive switching 'on' and 'off' does not reduce the amplitude.

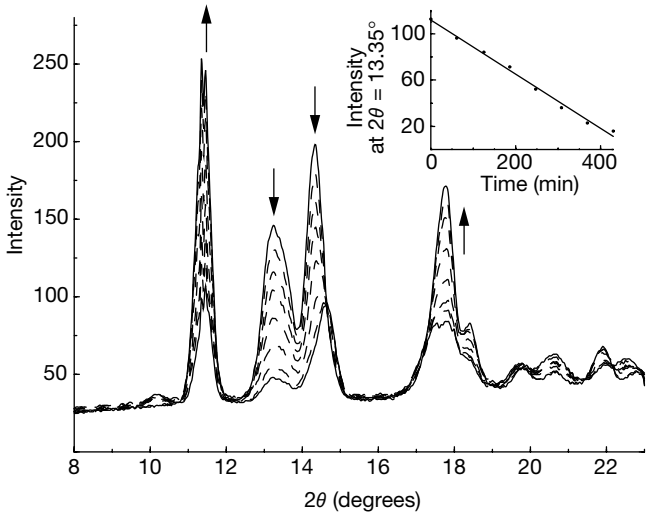

Figure 4 Time-resolved X-ray powder diffraction analysis of the transformation of crystalline **2** to **1** in an atmosphere of air. **2** was mounted in an open glass capillary on an Nonius Kappa charge-coupled device (CCD) diffractometer with Cu Kα radiation, graphite monochromator, λ = 1.5418 Å at a temperature of 293 K. Scans were performed every hour with a scan time of 6 minutes. After background subtraction, the characteristic intensities at 2θ = 11.33 (diagnostic for **1**) and 13.35 (for **2**) have been related to the reaction time. Inset, correlation exceeds 0.996 for a linear approximation.

signals is dependent on the atmospheric constitution and thus demonstrates the potential of this material as a crystalline switch (Fig. 3). The gas fixation process of crystalline **1** ('off' position) in a steady atmosphere of SO_2 is best approximated by a pseudo first-order rate law in organoplatinum species (that is, rate = k[Pt] where [Pt] is the concentration of **1**; Fig. 3), whereas a linear decrease of the characteristic absorption bands is noted when **2** ('on' position) is exposed to an inert gas. (In fact, k is (to our knowledge) the first reliable rate constant measured for the diffusion of a gas through a crystalline material. It is strongly temperature dependent: at a given particle size, the gas release is accelerated approximately fivefold when the temperature is raised from ambient (293 K) to 333 K and enormously retarded at low temperature (253 K, about 50 times slower). Preliminary measurements suggest that the gas desorption mechanism at higher temperatures may be different from that operating at ambient temperatures.) This suggests that in the rate-determining step of substrate binding, single platinum sites are involved. Although absorption of SO_2 on molecules which are located at the surface of the crystalline material is assumed to be facile, the transport of the gas into the interior of the crystal to neighbouring molecules is probably less favoured. This can be explained by considering competitive release of SO_2 back to the atmosphere. More importantly, incorporation of the substrate into the inner sphere is considerably complicated as an expansion of the crystal lattice occurs, involving, for example, reorganization of the relative position of the α-type networks (Fig. 2). This implies that building blocks containing bound SO_2 must influence their surrounding substrate-free neighbours in such a way that space is available for the gas molecule to move inside the densely packed supermolecule.

Using powder diffraction techniques, gradual transformation of **2** to **1** without formation of an intermediate has been observed, and the decrease of the intensity peaks of crystalline adduct **2** is accompanied by a proportional increase of the intensities assigned to **1** (see above, Fig. 4). Analysis of the characteristic intensities at low 2θ values strongly suggests a linear relationship between the change of the intensities and the elapsed time (see inset to Fig. 4), thus corroborating the results obtained from infrared spectroscopy (see above). Hence, a zero-order rate law is deduced for the release of SO_2 gas from crystalline **2**. The exact reaction rate is strongly dependent on the surface area of the sample (for example, particle size). Moreover, in a thin capillary, the desorption reaction of SO_2 from **2** proceeds considerably more slowly than in an open cup, but is still linear with time. This result emphasises the importance of area and the properties of the surface with respect to exchange with the local environment. Additionally, single crystals of **2** lose SO_2 primarily at the solid–gas interphase, resulting in the observation that a colourless zone 'grows' from the outside to the inside of the crystal block (Fig. 5). The desorption of SO_2 at the surface is assumed to be relatively fast and therefore the rate-determining step is presumably the diffusion-controlled transportation of the gaseous molecule from one metal centre to another, that is, the transfer of SO_2 from the core to the surface of the crystal.

The full reversibility of the crystalline-state absorption and desorption reaction is demonstrated by exposing a sample of regenerated **1** to atmospheres of air and SO_2 alternately. No loss in signal intensities, for example, owing to the formation of amorphous powder, is observed even after several repeated cycles. When single crystals of **2** are exposed to air, **1** is obtained as a colourless crystalline powder that is no longer suitable for a full single crystal X-ray analysis.

These results provide access to the preparation and engineering of efficient crystalline switches with unusual properties. The 'on/off' position of this switch may be defined, for example, by the crystal size and properties, or by the diagnostic colour of these materials. Most importantly, such switches are triggered primarily by their gaseous environment and may also be regulated by temperature. Owing to the insensitivity of the present organoplatinum systems towards light or oxidation[13–16], these materials have high potential for applications as gas sensors[29] and as photochemical switches in opto-electronic devices in, for example, data processing or non-linear optical technology. □

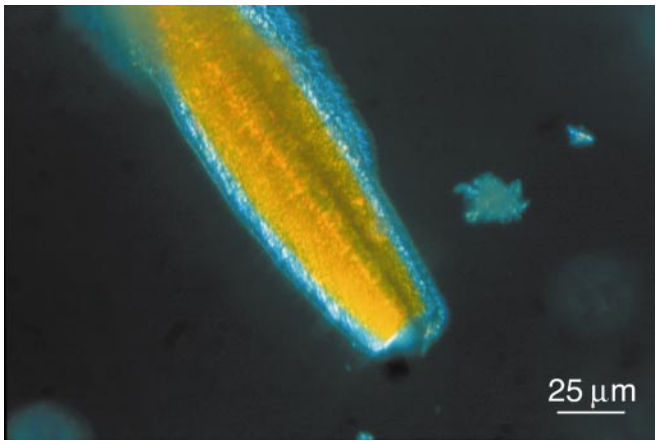

Figure 5 Formation of crystalline **1** from a single crystal of **2**. Shown after about 14 h in air, showing the colourless zone at the periphery and the orange colour in the core of the crystal.

Received 19 April; accepted 21 June 2000.

1. Fox, M. A. Fundamentals in the design of molecular electronic devices: long-range charge carrier transport and electronic coupling. *Acc. Chem. Res.* **32,** 201–207 (1999).
2. Kelly, T. R., De Silva, H. & Silva, R. A. Unidirectional rotary motion in a molecular system. *Nature* **401,** 150–152 (1999).
3. Koumura, N., Zijlstra, R. W. J., van Delden, R. A., Harada, N. & Feringa, B. L. Light-driven monodirectional molecular rotor. *Nature* **401,** 152–155 (1999).
4. Balzani, V., Gómez-López, M. & Stoddart, J. F. Molecular machines. *Acc. Chem. Res.* **31,** 405–414 (1998).
5. Sauvage, J. P. Transition metal-containing rotaxanes and catenanes in motion: toward molecular machines and motors. *Acc. Chem. Res.* **31,** 611–619 (1998).
6. Fabbrizzi, L., Licchelli, M. & Pallavicini, P. Transition metals as switches. *Acc. Chem. Res.* **32,** 846–853 (1999).
7. Collier, C. P. *et al.* Electronically configurable molecular-based logic gates. *Science* **285,** 391–394 (1999).
8. Liu, C. -Y. & Bard, A. J. Optoelectronic properties and memories based on organic single-crystal thin films. *Acc. Chem. Res.* **32,** 235–245 (1999).
9. Dunitz, J. D. in *Perspectives in Supramolecular Chemistry. The Crystal as a Supramolecular Entity* (ed. Desiraju, G. R.) 7 (Wiley, Chichester, 1996).
10. Albrecht, M., Gossage, R. A., Lutz, M., Spek, A. L. & van Koten, G. Diagnostic organometallic and metallodendritic materials for SO_2 gas detection: reversible binding of sulfur dioxide to aryl platinum(II) complexes. *Chem. Eur. J.* **6,** 1431–1445 (2000).
11. Chen, P., Wu, X., Liu, J. & Tan, K. L. High H_2 uptake by alkali-doped carbon nanotubes under ambient pressure and moderate temperatures. *Science* **285,** 91–93 (1999).
12. Dillon, A. C. *et al.* Storage of hydrogen in single-walled carbon nanotubes. *Nature* **386,** 377–379 (1997).
13. Ohashi, Y., Yanagi, K., Kurihara, T., Sasada, Y. & Ohgo, Y. Crystalline-state reaction of cobaloxime complexes by X-ray exposure. An order-to-order racemization in the crystal of [(*S*)-1-cyanoethyl](pyridine)-bis(dimethylglyoximato)cobalt(III). *J. Am. Chem. Soc.* **104,** 6353–6359 (1982).
14. Novak, K., Enkelmann, V., Wegner, G. & Wagener, K. B. Crystallographic study of a single crystal to single crystal photodimerization and its thermal reverse reaction. *Angew. Chem. Int. Edn Engl.* **32,** 1614–1616 (1993).
15. Kobatake, S., Yamada, T., Uchida, K., Kato, N. & Irie, M. Photochromism of 1,2-bis(2,5-dimethyl-3-thienyl)perfluorocyclopentene in a single crystalline phase. *J. Am. Chem. Soc.* **121,** 2380–2386 (1999).
16. Scheffer, J. R. & Pokkuluri, P. R. in *Photochemistry in Organized & Constrained Media* (ed. Ramamurthy, V.) 185 (VCH, New York, 1990).
17. Langeley, P. J. & Hulliger, J. Nanoporous and mesoporous organic structures: new openings for materials research. *Chem. Soc. Rev.* **28,** 279–291 (1999).
18. Estermann, M., McCusker, L. B., Baerlocher, C., Merouche, A. & Kessler, H. A synthetic gallo phosphate molecular sieve with a 20-tetrahedral-atom pore opening. *Nature* **352,** 320–323 (1991).
19. Hajdu, J. *et al.* Millisecond X-ray diffraction and the first electron density map from Laue photographs of a protein crystal. *Nature* **329,** 178–181 (1987).
20. Buss, C. E. *et al.* Structural investigations of vapochromic behavior. X-ray single-crystal and powder diffraction studies of $[Pt(CN\text{-}iso\text{-}C_3H_7)_4][M(CN)_4]$ for M = Pt or Pd. *J. Am. Chem. Soc.* **120,** 7783–7790 (1998).
21. Desiraju, G. R. *Crystal Engineering; The Design of Organic Solids* (Elsevier, Amsterdam, 1989).
22. Lehn, J.-M. *Supramolecular Chemistry: Concepts and Perspectives* (VCH, Weinheim, 1995).
23. van Koten, G. Tuning the reactivity of metals held in a rigid ligand environment. *Pure Appl. Chem.* **61,** 1681–1694 (1989).

24. Davies, P. J. *et al.* Organoplatinum building blocks for one-dimensional hydrogen-bonded polymeric structures. *Angew. Chem. Int. Edn Engl.* **35,** 1959–1961 (1996).
25. Braga, D., Grepioni, F. & Desiraju, G. R. Crystal engineering and organometallic architecture. *Chem. Rev.* **98,** 1375–1405 (1998).
26. Albrecht, M. & van Koten, G. Gas sensor materials based on metallodendrimers. *Adv. Mater.* **11,** 171–174 (1999).
27. Darensbourg, M. Y., Tuntulani, T. & Reibenspies, J. H. Structure/function relationships in ligand-based SO_2/O_2 conversion to sulfate as promoted by nickel and palladium thiolates. *Inorg. Chem.* **34,** 6287–6290 (1995).
28. Moffat, K. Time-resolved crystallography. *Acta Crystallogr. A* **54,** 833–841 (1998).
29. Kong, J. *et al.* Nanotube molecular wires as chemical sensors. *Science* **287,** 622–625 (2000).

Acknowledgements

We thank E. T. H. Lutz and A. M. M. Schreurs for technical assistance during the measurements and R. A. Gossage for discussions. This work was partially supported by the Council for Chemical Sciences from the Dutch Organization for Scientific Research (CW–NWO).

Correspondence and requests for material should be addressed to G.v.K. (e-mail: g.vankoten@chem.uu.nl).

Automatic design and manufacture of robotic lifeforms

Hod Lipson & Jordan B. Pollack

Computer Science Department, Volen Center for Complex Systems, Brandeis University, Waltham, Massachusetts 02454, USA

Biological life is in control of its own means of reproduction, which generally involves complex, autocatalysing chemical reactions. But this autonomy of design and manufacture has not yet been realized artificially[1]. Robots are still laboriously designed and constructed by teams of human engineers, usually at considerable expense. Few robots are available because these costs must be absorbed through mass production, which is justified only for toys, weapons and industrial systems such as automatic teller machines. Here we report the results of a combined computational and experimental approach in which simple electromechanical systems are evolved through simulations from basic building blocks (bars, actuators and artificial neurons); the 'fittest' machines (defined by their locomotive ability) are then fabricated robotically using rapid manufacturing technology. We thus achieve autonomy of design and construction using evolution in a 'limited universe' physical simulation[2,3] coupled to automatic fabrication.

In the field of artificial life, 'life as it could be' is examined on the basis of understanding the principles, and simulating the mechanisms, of real biological forms[4]. Just as aeroplanes use the same principles as birds, but have fixed wings, artificial lifeforms may share the same principles, but not the same implementation in chemistry. Stored energy, autonomous movement, and even animal communication are replicated in toys using batteries, motors and computer chips.

Our central claim is that to realize artificial life, full autonomy must be attained not only at the level of power and behaviour (the goal of robotics, today[5]), but also at the levels of design and fabrication. Only then can we expect synthetic creatures to sustain their own evolution. We thus seek automatically designed and constructed physical artefacts that are functional in the real world, diverse in architecture (possibly each slightly different), and automatically producible with short turnaround time, at low cost and in large quantities. So far these requirements have not been met.

The experiments described here use evolutionary computation for design, and additive fabrication for reproduction. The evolutionary process operates on a population of candidate robots, each composed of some repertoire of building blocks. The evolutionary process iteratively selects fitter machines, creates offspring by adding, modifying and removing building blocks using a set of operators, and replaces them into the population (see Methods section). Evolutionary computation has been applied to many engineering problems[6]. However, studies in the field of evolutionary robotics reported to date involve either entirely virtual worlds[2,3], or, when applied in reality, adaptation of only the control level of manually designed and constructed robots[7–9]. These robots have a predominantly fixed architecture, although Lund[10] evolved partial aspects of the morphology, Thompson[11] evolved physical electric circuits for control only, and we evolved static Lego structures, but had to manually construct the resultant designs[12]. Other works involving real robots make use of high-level building blocks comprising significant pre-programmed knowledge[13]. Similarly, additive fabrication technology has been developing in terms of materials and mechanical fidelity[14] but has not been placed under the control of an evolutionary process.

Our approach is based on the use of only elementary building blocks and operators in both the design and fabrication process. As building blocks are more elementary, any inductive bias associated with them is minimized, and at the same time architectural flexibility is maximized. Similarly, use of elementary building blocks in the fabrication process allows the latter to be more systematic and versatile. As a theoretical extreme, if we could use only atoms as building blocks, laws of physics as constraints and nanomanipulation for fabrication, the versatility of the manufacturable design space would be maximized. Earlier reported work that used higher-level components and limited architectures (such as only tree structures[2,3]) resulted in expedited convergence to acceptable solutions, but at the expense of truncating the design space. Furthermore, these design spaces did not consider manufacturability.

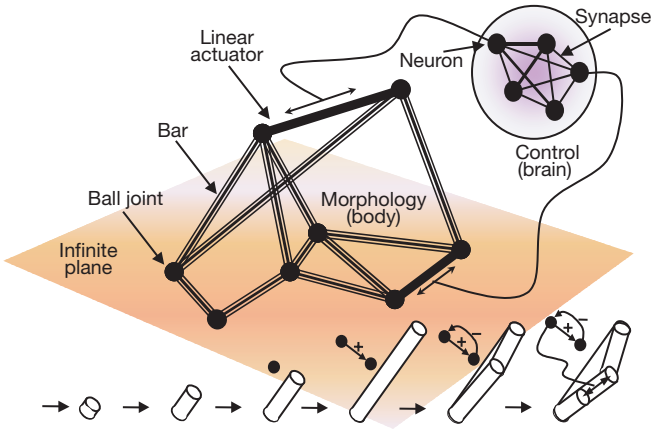

Figure 1 Schematic illustration of an evolvable robot. Bars connect to each other to form arbitrary trusses; by changing the number of bars and the way they connect, the structural behaviour of the truss is modified—some substructures may become rigid, while others may become articulated. Neurons connect to each other via synapses to form arbitrary recurrent neural networks. By changing the synapse weights and the activation threshold of the neuron, the behaviour of the neuron is modified. By changing the number of neurons and their connectivity, the behaviour of the network is modified. Also, we allow neurons to connect to bars: in the same way that a real neuron governs the contraction of muscle tissue, the artificial neuron signal will control the length of the bar by means of a linear actuator. All these changes can be brought about by mutational operators. A sequence of operators will construct a robot and its controller from scratch by adding, modifying and removing building blocks. The sequence at the bottom of the image illustrates an arbitrary progression of operators that create a small bar, elongate it and split it. Simultaneously, other operators create a neuron, add another neuron, connect them in a loop, and eventually connect one of the neurons to one of the bars. The bar is now an actuator. Because no sensors were used, these robots can only generate patterns and actions, but cannot directly react to their environment.